Journal of Coastal Research	SI	71	100–106	Coconut Creek, Florida	2014

Predicting Barrier Beach Breaching due to Extreme Water Levels at San Quntín, Baja California, Mexico

Teresa Vidal-Juárez [†*], Amaia Ruiz de Alegría-Arzaburu[†], Adán Mejía-Trejo[†], Héctor García-Nava[†], and Cecilia Enríquez [‡]

[†] Instituto de Investigaciones Oceanológicas
Universidad Autónoma de Baja California
Ensenada, México

[‡] Facultad de Ciencias,
Universidad Nacional Autónoma de México
Sisal, Yucatán, México

www.cerf-jcr.org

www.JCRonline.org

ABSTRACT

Vidal-Juárez, T.; Ruiz de Alegría-Arzaburu, A.; Mejía-Trejo, A.; García-Nava, H., and Enriquez, C., 2014. Predicting barrier beach breaching due to extreme water levels at San Quintín, Baja California, México. *In:* Silva, R., and Strusińska-Correia, A. (eds.), *Coastal Erosion and Management along Developing Coasts: Selected Cases.* Journal of Coastal Research, Special Issue, No. 71, pp. 100–106. Coconut Creek (Florida), ISSN 0749-0208.

This study comprises a first approach to numerically determine the hydrodynamic conditions leading to barrier breaching at San Quintín, located in the northwestern coast of the Baja California peninsula in Mexico. The barrier is backed by a large coastal lagoon, fronted by a field of submerged volcanoes located several kilometers off the coast and is exposed to large incoming wave energy dominated by the Pacific swell. The narrowest barrier beach sections are vulnerable to flooding due to overwash events that take place during concurrent high spring tides, energetic storm waves and a range of storm surge levels. Here, the conditions to barrier overwash and breaching occurrence are identified, and the extent of the floods is numerically quantified. For that purpose, the Delft3D hydrodynamic model is applied coupling waves and flows to simulate a series of scenarios, which comprise storm waves of different magnitudes and periods approaching from typical directions, and coupled to spring tides and several storm surge levels. As a consequence of the presence of submerged volcanoes off the coast, the incoming wave energy is mostly concentrated at two specific locations along the barrier beach, which correspond to the lowest and narrowest barrier locations. Due the large distance between both sites, longshore variations are not expected to be as strong as the cross-shore. Numerical results suggest that the barrier is susceptible to flooding during spring tides combined with extreme waves of significant wave heights larger than 3.5 m and a peak period of 7.5 s, and storm surge levels exceeding 0.9 m, which may lead to breaching.

ADDITIONAL INDEX WORDS: *Barrier breaching, overwash, submerged volcanoes.*

INTRODUCTION

Barrier beaches comprise natural coastal protection structures against flooding and water exchange between the sea and inland areas. Besides, the combination of extreme water levels and storm wave conditions can potential achieve the breaching of coastal barriers. A breach comprises a new permanent or intermittent water entrance formed due to erosion processes. Water scouring the barrier or quickly losing large volumes of sediment as slurry due to seepage effects are two ways of sandy barrier breaching occurrence (Kraus, 2002). Moreover, the lack of sediment available from the beach to landward often results in the degradation of the barrier crest relative to mean sea level (Bradbury, 2000).

Despite the complexity of the breaching process, efforts have been undertaken to quantitatively predict potential barrier breaching events (Bradbury, 2000; Sallenger, 2000; Kraus, 2002). Previous studies on barrier beach morphodynamics demonstrate the need of taking into account fundamental parameters such as the hydrodynamic processes (waves, storm surge and run-up conditions) and the barrier beach morphologic characteristics (sediment properties and beach profile shape) in order to accurately predict barrier breaching. When a decade of storm surge (S_{10}) data are available, and the diurnal tidal range is known (R), sandy barrier breaching can be predicted calculating the Breach Susceptibility Index (B) defined by Kraus (2002) as:

$$B = \frac{S_{10}}{R} \quad (1)$$

Field experiments have demonstrated the need of considering the spatial variability of barrier overwash processes to calculate net erosion or accretion across the beach profile. In addition, wave set-up must be included to adequately simulate cross-shore and longshore sediment transport processes during the breaching (McCall *et al*., 2010). Consequently, it is important to analyze the wave propagation from offshore to onshore to estimate the impact of nearshore waves on the coast (Roelvink *et al*., 2009; Salisbury, 2007). Low and flat landforms can function as submerged breakwaters dissipating large amount of the incoming wave energy (Gallop *et al*., 2012; Yamano *et al*., 2005). Likewise, local abrupt bathymetric changes such as nearshore submerged volcanoes can modify the incoming wave energy. Thus, the importance of determining wave propagation patterns across bathymetrically complex field sites.

DOI: 10.2112/SI71-012.1 received 3 April 2014; accepted in revision 6 July 2014.
*Corresponding author: vidal.teresa.uabc.edu.mx
© Coastal Education & Research Foundation 2014

Storm induced coastal flooding is considered one of the most common and widespread coastal hazards. Storms are predicted to be more intense and frequent in the future as a result of global warming and climate change. As existing climate models predict the acceleration of sea level rise, the increase of the water level should be coupled to existing models in order to improve the prediction of coastal flooding and barrier beach breaching (Pye and Blott, 2006). Most climate models predict a sea-level rise of about 0.4 to 0.7 m by the year 2100 for the northwestern Mexican coast (IPCC, 2007). In addition, the largest expected storm surge levels along the coast of California are ~ 0.8 m (Bromirski *et al*., 2003). Thus, future coastal morphodynamic models should include the combined effect of storm surge levels and sea level rise together with the storm wave conditions to assure an adequate prediction of the morphologic change on the coasts.

This study aims to numerically determine the hydrodynamic conditions leading to barrier breaching at San Quintín combining the effect of storm waves, storm surges and sea-level rise. The coastal lagoon within the research site comprises a highly productive ecosystem where a large number of oyster farms are established, hence, the relevance of predicting barrier breaching and the extent of the floods inland.

STUDY AREA

San Quintin beach, located in the northwest coast of the Baja California peninsula, Mexico, is part of a volcanic region (Figure 1). Submerged volcanoes are present ~7 km off the coast. Most of the volcanoes are less than 1 km in diameter and form a ~10 km long volcanic reef, parallel to the shore reaching a maximum water depth of 100 m. One of the volcanoes is emerged and forms the island of San Martin of ~2 km in diameter.

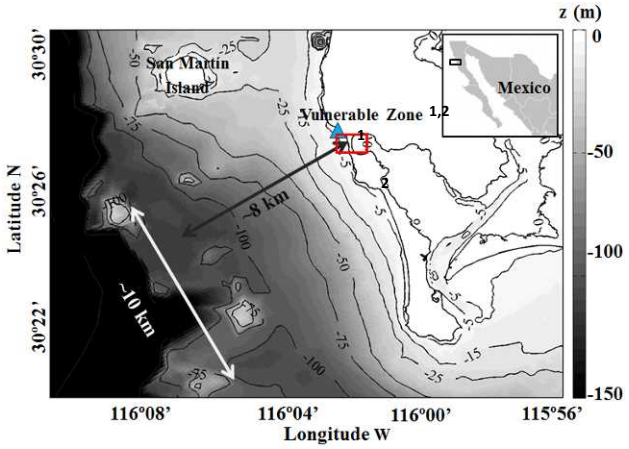

Figure 1. Location of San Quintin within Mexico (top right panel) and the offshore and nearshore bathymetry. The most vulnerable location for barrier breaching (red box) and the location of the meteorological station (blue triangle) are shown.

The barrier beach is ~12 km long of a ranging width of 200-800 m and backed by a coastal lagoon (Figure 2). Several volcanoes joint by sandy dunes separate the beach from the lagoon. The beach is primarily sandy except from the presence of a layer of gravel and pebbles at some specific locations.

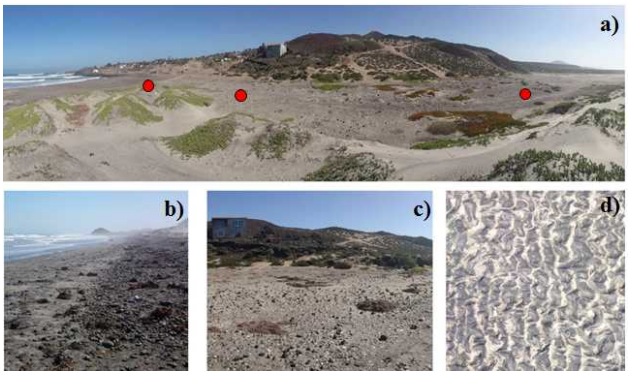

Figure 2. (a) Overview of the barrier breaching location in the northwestern San Quintín barrier beach (location marked by a rectangle in Figure 1). The red dots show the locations from where the pictures below were taken. (b) The beach face which is usually sandy and sometimes covered by gravel and pebbles. (c) Compacted sand and few pebbles can be found along the supratidal beach. (d) Ripples identified across the overwash locations towards the lagoon.

Barrier beach breaching occurred across the narrowest beach section sometime between the late 70's and early 80's after a sequence of extreme storm events (Pers. Comm. local oyster farmer). Since then, the dune has not recovered, thus, this is a vulnerable location to forthcoming storm induced flooding.

San Quintin beach is microtidal, with mean spring and neap tidal ranges of 2.5 m and 1 m, respectively. The most frequent winds are northwesterlies of maximum and mean magnitudes of 9 and 4 m/s, respectively (Gil-Silva *et al*., 2012). The incoming waves are dominated by northwesterly swell except to southwesterly waves which are typical during the summer.

METHODOLOGY

The Delft3D model is applied to propagate offshore waves towards the nearshore and couple them with the storm surge and tidal conditions. This model has been previously applied to determine nearshore sediment transport and hydrodynamic processes at similar research sites (Choi and Lee, 2004; Dissanayake and Wurpts, 2013) and proved to provide accurate hydro- and morpho-dynamic results.

Conceptual Aspects of the Delft 3D Model

The Delft3D model couples the wave and flow modules to a local bathymetric grid. Based on a local bathymetry which includes the coastline and other coastal bodies, the grid module is used to compute the model domain.

The wave module computes the wave propagation based on the third-generation Simulating WAves in the Nearshore (SWAN) spectral model by solving the wave action balance

equation (Booij *et al*., 1999). The Flow module is based on the conservation of mass and momentum, expressed as the continuity equation:

$$\frac{\partial u}{\partial x}+\frac{\partial v}{\partial y}+\frac{\partial w}{\partial z}=0 \quad (2)$$

and the shallow water horizontal water movement equations (eq. 3 and 4), which are solved by the implicit ADI factorization method (Alternating Direction Implicit) using a staggered grid (Arakawa C-grid) based on initial model conditions.

$$\frac{\partial u}{\partial t}+u\frac{\partial u}{\partial x}+v\frac{\partial u}{\partial y}+w\frac{\partial u}{\partial z}-fv = -\frac{1}{\rho_0}P_x+F_x+\frac{\partial}{\partial z}\left(v_V\frac{\partial u}{\partial z}\right)+M_x \quad (3)$$

$$\frac{\partial v}{\partial t}+u\frac{\partial v}{\partial x}+v\frac{\partial v}{\partial y}+w\frac{\partial v}{\partial z}+fu = -\frac{1}{\rho_0}P_y+F_y+\frac{\partial}{\partial z}\left(v_V\frac{\partial v}{\partial z}\right)+M_y \quad (4)$$

where u and v are the horizontal velocity under the x and y axis respectively. The vertical speed is denoted by w in the z axis. The eddy viscosity is described as v_V. The pressure gradients (barotropic and baroclinic) are represented by P_x and P_y, respectively. F_x and F_y represent the Reynolds stress in the momentum equations. M_x and M_y are the contributions due to external sources, f is the Coriolis parameter and ρ_0 the water density.

The model has an additional morphologic module to simulate morphological changes due to sediment transport, and is based on the advection and diffusion processes of suspended sediment (Hydro-Morphodynamics, 2011). This is solved with the sediment mass balance equation as follows:

$$\frac{\partial c}{\partial t}+\frac{\partial uc}{\partial x}+\frac{\partial vc}{\partial y}+\frac{\partial (w-w_s)c}{\partial z}-\frac{\partial}{\partial x}\left(\epsilon\frac{\partial c}{\partial x}\right)-\frac{\partial}{\partial y}\left(\epsilon\frac{\partial c}{\partial y}\right)-\frac{\partial}{\partial x}\left(\epsilon\frac{\partial c}{\partial z}\right)=0 \quad (5)$$

where c is the mass concentration of sediment transport, w is the flow velocity components, ϵ is the sediment's eddy diffusivity and w_s the sediment setting velocity.

Model Grid, Topography and Bathymetry

The model bathymetry was referred to the low mean sea level (LMSL) and determined using data of different spatial resolution. The Etopo1 Global Relief Model (Amante y Eakins, 2009) dataset was used for the offshore extent and the Mexican Navy (EUM Secretaría de Marina, 2008) data were acquired for the coastal lagoon and nearshore area. Additional topographic data were obtained from Valdéz-Martínez (2012), which comprised of largely spaced beach profiles (~ 1km apart) measured along the barrier beach using a total station.

A curvilinear mesh of varying resolution from 50 to 300 m was selected for the computational grid. Due to the lack of nearshore wave measurements at San Quintín, the domain was extended 11 km off the coast where offshore wave conditions were set as boundary. A higher resolution grid of 35 to 55 m was defined in the nearshore area to provide detailed outputs on the barrier beach hydrodynamics; this grid was nested into the larger one.

Boundary Conditions

The model was forced by wind, wave and tidal conditions for a period of two weeks at time steps of 30 seconds. The tidal data included spring and neap tides and were obtained from a tidal prediction model (from CICESE, Mexico). *In-situ* wind data were obtained from an Aanderaa meteorological station located in the study site, which operates since 2002 (see the triangle in Figure 1).

The offshore wave boundary conditions (see thick line in Figure 3) were defined combining measurements collected from the NOAA 46047 buoy with a data of full wave directional spreading from the PACE/IOWAGA (PACifico Este-/Integrated Ocean Waves for Geophysical and other Applications) wave hindcast (Rascle and Ardhuin, 2013).

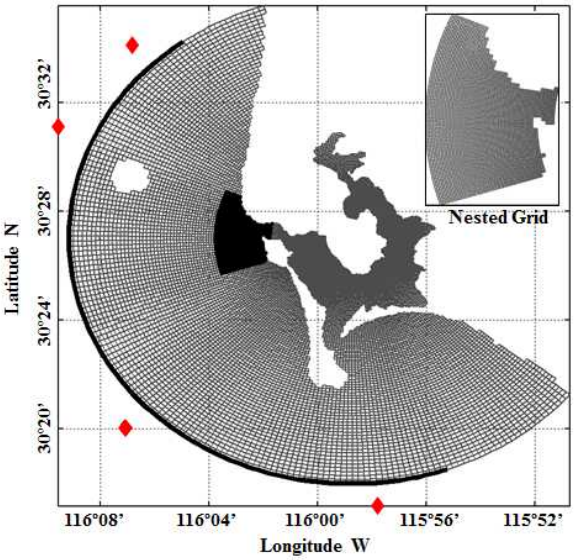

Figure 3. Large grid and nested grid used to propagate waves and flows. The coastal boundary is closed and the ocean boundary is opened with absorbance characteristics. The thicker line represents the opened offshore boundary forced with tides and wave conditions. Diamonds are linked to sites of observational wave data from the PACE grid.

Wave data from the IOWAGA hindcast from 2008 to 2013 indicates the dominance of northwesterly swell with mean significant wave height of 1.5 m, peak period of 7 s and a nautical direction of 277º (Figure 4). Southwesterly swell is more frequent in summer. Based on the existing offshore wave data, storms were defined as events of significant wave heights exceeding 2.4 m (twice the standard deviation) and with a minimum duration of 12 hrs. For the six year period, a total

amount of 31 storms were identified, with an average occurrence of 5 storms per year. At least one storm with a minimum duration of 2 days took place each year, and the storm with the largest duration was of 4.5 days.

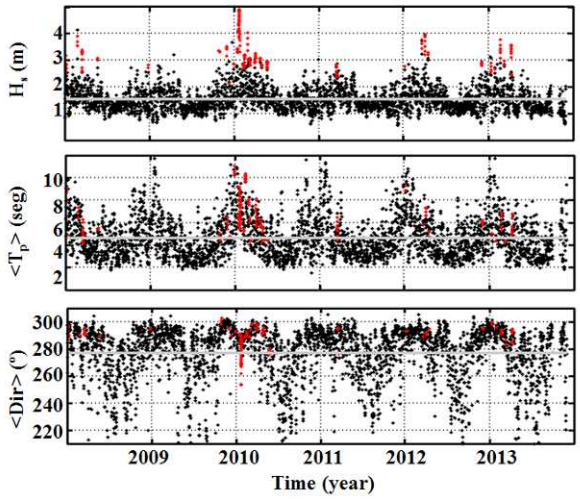

Figure 4. Daily significant wave height, mean peak period and wave directions from 2008 to 2013 obtained from the IOWAGA hindcast at a grid cell of 600 – 900 m water depth (see ◆ in Figure 3). Larger waves than 2 meters lasting for more than 12 hours define the storm events (marked by dark dots).

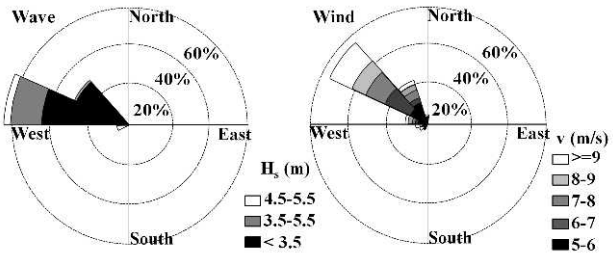

Figure 5. Wave rose (left panel) representing offshore storm wave conditions from the IOAWAGA hindcast at a grid cell ~11km off the coast (see ◆ in Figure 3) and wind rose (right panel) showing storm wind conditions registered at the meteorological station (see ▲ in Figure 1) from 2008 to2013.

The storms identified from 2008 to 2013 were dominated by northwesterly waves and characterized by mean H_s of 3 m and T_p of 8 s (Figure 4). The most extreme waves were northwesterly directed and of a maximum H_s of 5 m and T_p of 9 s. The wind was predominantly northwesterly during the storms and of an average speed of ~7.5 m/s, whereas the strongest wind was northerly directed and had an average speed larger than 9 m/s.

In order to couple the tides with the local set-up, storm surges were calculated for a period from November 2013 to February 2014 (Figure 6). During that period of time, limited by data availability, the storm surge levels ranged from 0.1 to 0.2 m for the largest identified northwesterly storm (28th of February 2014) characterized by an average wave height of 1.85 m and a peak period of 11 s. In comparison to the storms identified over a larger period of time (Figure 5), this storm is considered weak, thus, the obtained storm surge level is set as low.

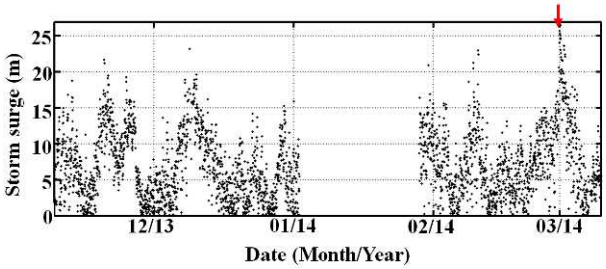

Figure 6. Time series of storm surges calculated from the difference between the measured and the astronomic tides (predicted from the CICESE model, Mexico) from November 2013 to February 2014.

In order to numerically determine the hydrodynamic conditions that lead to a potential breaching of the barrier, different test cases were set varying the forcing boundary conditions such as the water levels from 0 to 1 m (simulating a range of storm surge levels) for different wave conditions (H_s, T_p and directions) represented on the wave rose, and the wind forcing was set as constant (Table 1).

Table 1. *Hydrodynamic conditions for different storm events simulated with Delft3D.*

Case	Wave parameters			Wind parameters		Storm Surge
	Hs	Tp	Dir	V	Dir	Rising
	[m]	[s]	[°]	[m/s]	[°]	[m]
1	5	7	265	8	280	0
2	5	7	265	8	280	1
3	5	8	275	8	280	0.8
4	5	8	275	8	280	0.9
5	5	8	275	8	280	1
6	3.5	8	275	8	280	1
7	3.5	8	285	8	280	0
8	3.5	8	285	8	280	1

RESULTS

Wave propagation results show the complexity of the patterns of the incoming waves, which is attributed to the presence of the submerged volcanoes. After the pass of waves over the volcanoes, the wave energy focuses at different alongshore barrier locations. The location of the focusing of the wave energy depends on the incident wave direction. Modeling results indicate that the wave focusing occurs at the locations where the barrier levels are the lowest (Figure 7) and barrier breaching is expected to occur, either for northwesterly or southwesterly storm waves. Southwesterly waves are able to concentrate

higher energy than northwesterly waves. At 4 m water depth, southwesterly swell waves are of ~3 m height and the northwesterly directed of ~2.5 m.

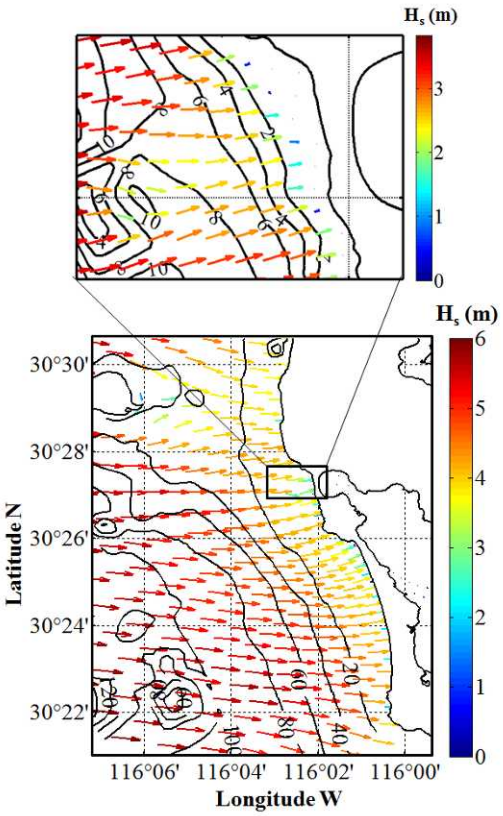

Figure 7. Wave propagation results from the Delft3D model for the most frequent storm waves of H_s of 5 m, T_p 8 s and a wave direction of 275° at boundary condition. The top panel is a close up of the bottom panel for the barrier breaching location.

The conditions for barrier breaching occurrence were established considering the combined effect of tides and waves. The barrier breaches when the water level exceeds 2 m, which takes place during high spring tides combined with and additional increase of 0.9 m due to the wave set-up and storm surge (Figure 8). The numerical results depend on the computational cell size (~35 m), which may induce quantitative inaccuracies across the narrowest barrier locations; nevertheless, they suggest a realistic perspective for the flooding extent and occurrence. Numerical outputs indicate that during the breaching, the water flows towards the low-lying regions.

DISCUSSION

Wave Propagation

The submerged volcanoes would be expected to dissipate a large amount of the incoming wave energy. Numerical results, however, indicate that they rather focus the wave energy at some specific sites along the barrier. Gallop (1990) and Yamano (2005), among others, indicate that submerged structures should be flat in order to serve as breakwaters; otherwise, these structures may concentrate the wave energy onshore because of the refraction processes. Thus, the focusing effect could be due to the craters of the volcanoes being of conical shaped rather than flat.

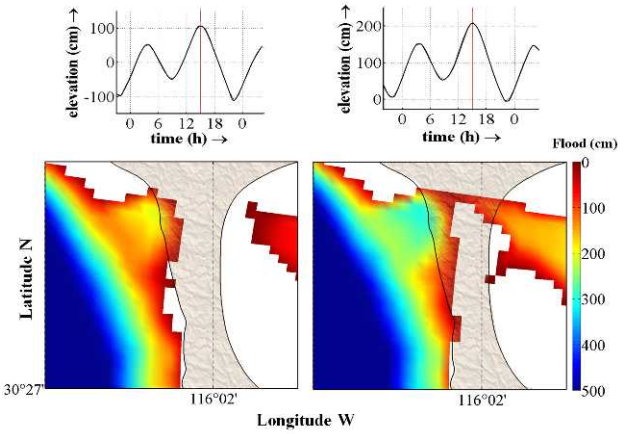

Figure 8. Barrier overtopping and overwashing during high spring tides and extreme wave conditions of H_s of 5 m, T_p of 8 s from 275° without storm surge (left panel) and for the same conditions and 1 m of storm surge (right panel). The modeled area corresponds to the rectangle in Figure 1.

Breaching and Flooding

Although flood events did not occur for typical storm surge values for the Californian coast (Bromirski *et al.*, 2003), there is evidence of flooding at the narrowest and lowest site of the barrier. In addition to the testimony of the local fishermen, pebbles and gravel can be found along the lowest parts of the barrier remaining from previous washovers (Figure 2c). Overwashing events seemed to have carried coarse material across the barrier crest. In addition, ripples of compacted sediment are present across the overwash locations towards the lagoon (Figure 1d), which indicate the presence of past floods and barrier beaching occurrence.

The modelling tests to calculate the extent of floods were solely established using the hydrodynamic forcing, which comprised the incoming wave energy coupled to tidal and storm surge levels for a constant wind forcing. Nonetheless, longshore and cross-shore sediment transport processes interfere with the incoming hydrodynamics and at conditions of an absence in sediment supply, the hydrodynamic forcing could largely erode the barrier crest (Bradbury, 2000). In addition, morphologic changes of the barrier crest will interfere with the beach morphodynamics. Thus, it is a relevant matter to couple the sediment transport processes with the hydrodynamic forcing, in order to fully run the morphodynamic model and enable an adequate evaluation of barrier beach overwashing events, and the breaching extent. If the degradation of the barrier persists, due to the impact of a sequence of future storm events, or the

anthropogenic extraction of sediment on the beach, barrier overwashing and inland flooding will become frequent. Hence, future work aims to numerically predict barrier breaching considering the morphodynamic processes.

Findings

The numerical results obtained on this study will comprise an input to further research on barrier beach morphodynamics at San Quintín. The obtained hydrodynamic thresholds that lead to breaching will be set as boundary conditions to carry out additional morphodynamic model simulations with XBeach. Further modeling efforts need to account for higher resolution bathymetric and topographic data. These results revealed the sensitivity of the numerical model to the grid resolution; hence, the importance of integrating a more detailed topographic and bathymetric data to obtain more accurate outputs.

Since long-term barrier beach morphodynamics is dependent on sea level rise, sediment transport, sediment supply, the incident hydrodynamic conditions and barrier geometry (Bradbury, 2000), these variables will be further considered on the morphodynamic numerical model to carry out a comprehensive study on the processes that induce barrier breaching.

Due to the absence of historical data, storm impacts have not yet been measured. Thus, there is a need of measuring wave and tidal data to enable the calculation of the storm surge levels for different wave and wind conditions. Moreover, detailed pre- and post-storm topographic and bathymetric measurements would be needed to determine the vulnerability to breaching of the barrier beach.

CONCLUSIONS

As a consequence of the presence of submerged volcanoes off the coast, the incoming wave energy at San Quintín is mostly concentrated at two specific locations along the barrier beach, which correspond to the lowest and narrowest barrier locations. On those locations, numerical results suggest that the barrier beach is susceptible to flooding during high spring tides combined with extreme wave conditions (wave heights larger than 3.5 m and 7.5 second of peak period) and storm surge levels exceeding 0.9 m, which may lead to barrier breaching.

ACKNOWLEDGMENTS

This publication is one of the results of the Latin American Regional Network global collaborative project ‘‘EXCEED – Excellence Center for Development Cooperation – Sustainable Water Management in Developing Countries’’ consisting of 35 universities and research centres from 18 countries on 4 continents. The authors would like to acknowledge the support of the German Academic Exchange Service DAAD, the Centro de Tecnologia e Geociências da Universidade Federal de Pernambuco, the Fundação de Amparo a Ciência e Tecnologia do Estado de Pernambuco-FACEPE and the Instituto de Ingeniería of the Universidad Nacional Autónoma de México for their participation in this EXCEED project.

The first author is grateful for the support given by CONACyT through an MSc scholarship. The Mexican Navy (Secretaria de Marina) is acknowledged for providing offshore and nearshore bathymetric data for the field site. Thanks are extended to Dr. Oscar Eduardo Delgado Gonzalez for providing topographic data.

LITERATURE CITED

Amante, C., and B.W. Eakins, 2009. ETOPO1 1 Arc-Minute Global Relief Model: Procedures, Data Sources and Analysis. *NOAA Technical Memorandum NESDIS NGDC-24*. National Geophysical Data Center, NOAA.

Booij, N.; Ris, R.C., and Holthuijsen, L.H., 1999. A third-generation wave model for coastal regions. 1. Model description and validation. *Journal of Geophysical Research* 104, 7649–7666.

Bradbury, A.P., 2000. Predicting breaching of shingle barrier beaches - recent advances to aid beach management. *Proceeding of the 35th MAFF Conference of River and Coastal Engineers* 5(3), 1-13.

Bromirski, P.D.; Flick, R.E., and Cayan, D.R., 2003. Storminess variability along the California coast: 1858-2000. *Journal of Climate* 16(6), 982-993.

Choi, K.W., and Lee, J.H.W., 2004. Numerical determination of flushing time for stratified water bodies. *Journal of Marine Systems* 50(3-4), 263–281.

Dissanayake, D., and Wurpts, A., 2013. Modelling an anthropogenic effect of a tidal basin evolution applying tidal and wave boundary forcings: Ley Bay, East Frisian Wadden Sea. *Coastal Engineering* 82, 9–24.

EUM Secretaría de Marina, dirección general de investigación y desarrollo costa oeste, 2008. Bahía Santa María B. C. In *Carta SM-121.1, Datum WGS-84*, 1st. Ed. Dic.2004/ REIMP.CORR. A. M.

Gil-Silva, E.; Delgado-González, O.E., and Mejía-Trejo, A., 2012. *Informe de datos meteorológicos de la estación la Chorera, San Quintín, B.C. Technical report*, 4-46 (in spanish).

Gallop, S.L.; Bosserellea C.; Eliot, I., and Pattiaratchi, C.B., 2012. The influence of limestone reefs on storm erosion and recovery of a perched beach. *Continental Shelf Research* 47, 16–27.

Hydro-Morphodynamics, 2011. *Delft3D-FLOW Simulation of multi-dimensional hydrodynamic flows and transport phenomena, including sediments*. In Delft3D User Manual, Copyright © 2011 Deltares, 20-70.

IPCC, 2007. Cambio climático 2007, informe de síntesis. In *Intergovernmental Panel on Climate Change*, Geneva, Switzerland (in spanish).

Kraus, N., 2002. *Barrier Breaching Processes and Barrier Spit Breach, Stone Lagoon, California*, *Shore and Beach*, 70(4).

McCall1, R.T.; Plant, N.G., and van Thiel de Vries1 J.S.M., 2010. The effect of longshore topographic variation on overwash modeling. *In*: Proceedings *32nd International Conference on Coastal Engineering* (Shanghai, China), p. sediment.36.

Pye, K., and Blott, S., 2006. Coastal processes and morphological change in the Dunwich-Sizewell area, Suffolk, UK. *Journal Coastal of Research* 22(3), 453-473.

Rascle, N. and Ardhuin, F., 2013. A global wave parameter database for geophysical applications. Part 2: model validation with improved source term parameterization, *Ocean Modelling*, 70(10), 145.

Roelvink, D.; Reniers, A.; van Dongeren, A.; van Thiel de Vries, J.; McCall, R., and Lescinski J., 2009. Modelling storm impacts on beaches, dunes and barrier islands. *Coastal Engineering* 56, 1133– 1152.

Sallenger, A.H. Jr., 2000. Storm impact scale for barrier islands, *Journal of Coastal Research*, 16(3), pp. 890-895.

Salisbury, M.B. and Hagen S., 2007. The effect of tidal inlets on open coast storm surges hydrographs. *Coastal Engineering* 54, 377-391.

Valdez-Martínez, E.S., 2012. *Identificación de las zonas de riesgo ante el aumento paulatino del nivel medio del mar como posible insumo para el manejo de la acuacultura y el turismo de Bahía San Quintín en Baja California, México* (unpublished master's thesis*)*. Autonomous University of Baja California, Ensenada, Baja California, México.

Yamano, H.; Kayanne, H., and Chikamori, M., 2005: An overview of the nature and dynamics of reef islands. *Global Environmental Research* 9(1), 9–20.